

The role of surface Zn²⁺ ions in the transesterification of vegetable oils over ZnO supported on Al₂O₃ and Fe₂O₃†

Cite this: *Catal. Sci. Technol.*, 2014, 4, 851

K. Thirunavukkarasu,^{*a} T. M. Sankaranarayanan,^{ab} A. Pandurangan,^b R. Vijaya Shanthy^a and S. Sivasanker^a

Samples of ZnO–Al₂O₃ and ZnO–Fe₂O₃ with different loadings of ZnO (5–20 wt%) were prepared by impregnation of the supports (γ -Al₂O₃ and α -Fe₂O₃) with ZnNO₃ and calcination at 873 K. XRD studies of the calcined samples revealed that the ZnO had reacted with the support to form the corresponding spinels, ZnAl₂O₄ and ZnFe₂O₄. The catalytic activity of the supported spinel samples, and samples of stoichiometric ZnAl₂O₄ and ZnFe₂O₄ prepared by co-precipitation were examined for the transesterification of sunflower oil, waste cooking oil and Jatropha oil. Linear relationships between the spinel content, estimated by XRD, and surface Zn concentration estimated by XPS and transesterification activity of the samples were obtained. XVB (X-ray valence band) studies provided evidence to suggest that the Zn 3d electrons may have played a major part in the electronic excitation of the spinels (ZnAl₂O₄ and ZnFe₂O₄) and, therefore, their catalytic activity.

Received 29th October 2013,
Accepted 2nd December 2013

DOI: 10.1039/c3cy00857f

www.rsc.org/catalysis

1. Introduction

Fatty acid methyl esters (FAME; biodiesel), the key product from the transesterification of vegetable oils, are among the important renewable transportation fuels in use today. Their increased use is expected to decrease the rate of CO₂ build up in the atmosphere. The transesterification of vegetable oils is at present mostly carried out using soluble alkali catalysts. The disadvantages of using alkali catalysts are soap formation, poor quality of the glycerol byproduct, wastewater generation and non-suitability for oils containing free fatty acids (FFA). Among the many solid catalysts which have been reported^{1–5} as alternatives to the homogeneous acid catalysts, a ZnAl₂O₄ based catalyst was developed for the transesterification by the Institut Francais du Petrole (IFP) and was commercialized by Axens.^{6,7}

ZnAl₂O₄ belongs to the AB₂O₄ spinel oxides and possesses good thermal stability, no/very little leaching during reactions, hydrophobicity and ease of preparation with large external areas. Apart from transesterification, ZnAl₂O₄ is known to be active as a heterogeneous catalyst for reactions like dehydration, hydrogenation, dehydrogenation, cracking, synthesis of fine chemicals^{8–13} and in photocatalytic reactions.^{14,15}

ZnFe₂O₄, another important candidate in the AB₂O₄ spinel oxides, is reported to be an active heterogeneous catalyst for *N*-alkylation reactions,^{16,17} the water gas shift reaction,¹⁸ *O*-acylation,¹⁹ the oxidative dehydrogenation of *n*-butane,^{20,21} and as a photocatalyst for water splitting reactions,²² the decomposition of organic pollutants²³ and hydrogen production.²⁴ In AB₂O₄ spinel oxides, more octahedral sites are exposed on the surface than tetrahedral sites according to Low Energy Ion Scattering (LEIS) studies,^{25,26} *i.e.*, more B atoms are present on the surface than A atoms.

After the Axens process, many reports on ZnAl₂O₄ catalysts for the transesterification of vegetable oils started to emerge in the literature.^{27–31} Many of them mainly deal with the engineering aspects of the process and reveal the importance of large surface area and pores. Jiang *et al.*²⁹ observed that the transesterification reaction on Zn/Al mixed oxide catalysts was more feasible due to its basic sites. Liu *et al.*³⁰ reported that strong basicity and large pores were beneficial for the La-loaded ZnAl₂O₄ catalysed transesterification reaction. They found that a La-loading of 5.5 wt% showed the highest activity though they had strongly basic catalysts with higher La-loadings. To contradict these studies, a recent literature report on the transesterification reaction has revealed that the ZnAl₂O₄ surface contains more acidic sites than basic sites.³¹

The interaction of ZnO with γ -Al₂O₃ or α -Fe₂O₃ supports has been reported in the literature. Strohmeier and Hercules³² observed that Zn²⁺ ions interact strongly with the γ -Al₂O₃ support for >20% loadings of ZnO to form surface spinels. An electronic interaction between Zn²⁺ and Fe³⁺ ions of

^a National Centre for Catalysis Research, Indian Institute of Technology, Chennai-600 036, India. E-mail: KThirunavukkarasu@gmail.com; Tel: +91 44 22574238

^b Department of Chemistry, Anna University, Chennai-600 025, India

† Electronic supplementary information (ESI) available. See DOI: 10.1039/c3cy00857f

ZnFe₂O₄-ZnO catalysts was observed through Mossbauer spectroscopy by Armendariz *et al.*²¹ though the Zn²⁺ ions were not involved directly in the oxidative dehydrogenation reaction of *n*-butane. Unfortunately, the authors could not observe the same interaction with Fe₂O₃-ZnFe₂O₄ catalysts as Zn is inactive in Mossbauer spectroscopy. The role of Zn-ions in spinel catalysis has been recognised in the following studies. Sreekumar and Sugunan studied alkylation reactions of Zn-Co mixed ferrites and observed that the catalyst with a ratio with more Zn²⁺ content is more active and selective for the *N*-methylation reaction of aniline.¹⁷ Vijayaraj and Gopinath¹⁶ observed an active spacer role of the Zn²⁺ ions for the *N*-methylation reaction on Zn-Cu mixed ferrites and a stabilizer role of the Zn²⁺ ions towards the Cu²⁺ ions during the reaction, from XPS studies.

We now present our studies on the catalytic activity of ZnO supported on γ -Al₂O₃ and α -Fe₂O₃ in the transesterification of vegetable oils, *viz.* sunflower oil, waste (used) sunflower oil and Jatropha oil, carried out as part of our ongoing research on the transesterification of vegetable oils with solid oxide catalysts and spinel oxides.^{33,34} Samples of ZnO-Al₂O₃ and ZnO-Fe₂O₃ containing different amounts of ZnO were prepared by impregnation, characterized by physicochemical methods and their activities for the transesterification with methanol of sunflower oil, waste cooking oil and Jatropha oil were evaluated in a batch reactor. XPS studies reveal the active role of Zn-ions in the transesterification reactions.

2. Experimental section

2.1. Materials used and preparation of catalysts

Cooking grade sunflower oil, waste (used) sunflower oil and Jatropha oil were procured locally. Their fatty acid compositions are reported in Table 1. Methanol (AR Grade; SRL, India) was distilled and dried over a molecular sieve (4 Å) prior to use.

Samples of ZnO-Al₂O₃ and ZnO-Fe₂O₃ with different loadings of ZnO (5–20 wt%) were prepared by impregnation of the supports (γ -Al₂O₃ and α -Fe₂O₃) with ZnNO₃, drying in air (353 K; 12 h) and calcining at 873 K (6 h). Additionally, spinels of ZnAl₂O₄ and ZnFe₂O₄ were prepared by mixing stoichiometric amounts of the required metal nitrate solutions (1 : 2 mole ratio; 40 ml) and adding rapidly to a solution of NH₄OH (25 wt%; vol. 25 ml) at room temperature (300 K) under constant and vigorous stirring. The precipitates were

aged for 12 hours and dried at 353 K in an air oven for about 12 hours. The dried materials were powdered and calcined at 873 K for 6 h. The stoichiometric spinels are represented by the general formula ZnB₂O₄, where B is Al or Fe, and the non-stoichiometric mixed oxides are represented by *n*ZnB, where *n* represents the wt% of ZnO loading in the support.

2.2. Characterization of supports and catalysts

X-ray diffraction (XRD) patterns of the calcined materials were obtained using a Rigaku Miniflex II with Cu K α radiation. The phases were identified by matching of the peaks with JCPDS (Joint Committee on Powder Diffraction Standards) data files. Surface area determination was performed by the BET method (Micromeritics ASAP 2020). Before analysis the samples were degassed at 623 K for 8 to 10 h. The acidity of the samples was measured by the temperature-programmed desorption (TPD) of ammonia (AutoChem 2910, Micromeritics, USA). The standard procedure for the TPD measurements involved the activation of the sample in flowing He at 873 K (1 h), cooling to 323 K, adsorbing NH₃ from a He-NH₃ (10%) mixture, desorbing in He at 323 K for 30 min, and finally carrying out the TPD experiment by raising the temperature of the catalyst in a programmed manner (10 K min⁻¹). The areas under the TPD curves were converted into meq NH₃ per gram of catalyst based on injection of known volumes of the He-NH₃ mixture under similar conditions.

Diffuse reflectance UV-Vis spectra of the powder samples were recorded on a Thermoscientific Evolution-600 spectrometer. BaSO₄ (spectral grade) was used as a reference material. XPS measurements were carried out using a multi-probe system (Omicron Nanotechnology, Germany) equipped with a dual Mg/Al X-ray source and a hemispherical analyzer operating in constant analyzer energy (CAE) mode. The spectra were obtained with a 50 eV pass energy for the survey scan and 20 eV for individual scans. The Mg K α X-ray source was operated at 300 W and 15 kV. The base pressure in the analyzing chamber was maintained at 1 \times 10⁻¹⁰ mbar. The data were processed with the Casa XPS program (Casa Software Ltd., U.K.). The peak areas were determined by integration employing a Shirley-type background. Peaks were considered to be a mix of Gaussian and Lorentzian functions in a 70/30 ratio. The peaks were calibrated by taking the adventitious carbon's C 1s line as 284.9 eV. Fourier transform infrared (FT-IR) spectra for the samples were recorded using a Bruker Tensor-27 instrument.

Table 1 Composition of the vegetable oils

Fatty acid composition [%]	Sunflower oil	Waste cooking oil	Jatropha oil
Palmitic acid (C _{16:0})	6.5	6.3	17.9
Stearic acid (C _{18:0})	0.5	0.5	7.3
Oleic acid (C _{18:1})	22.5	21.9	41.8
Linoleic acid (C _{18:2})	70.5	68.8	25.0
Free fatty acids (FFA)	—	2.5/[C ₁₆ , 0.2; C _{18:1} , 0.9; C _{18:2} , 1.4]	8.0/[C ₁₆ , 2.0; C _{18:1} , 3.2; C _{18:2} , 2.4; C ₁₈ , 0.4]

2.3. Transesterification of vegetable oils

The catalytic activity of the samples was evaluated in an SS batch reactor (Parr, USA; 300 ml) at different run durations (2–10 h) and at different temperatures (393–453 K) using 1 g of finely ground catalyst (passing through ASTM 200 Mesh). The amount of oil used was 20 g; the amount of methanol used depended on the required oil/methanol mole ratio. The stirring speed for all the runs was maintained at 600 rpm. At the end of the desired reaction time, the autoclave was cooled to room temperature, the product was diluted with water (100 ml), and the catalyst was removed by filtration. The two liquid layers were separated using a separating funnel, the lower layer consisting of water, glycerol and methanol and the upper one containing fatty acid alkyl esters, unreacted oil and intermediate products.

2.4. Product analysis

The product composition was determined by analyzing the oil layer in a gas chromatograph (Perkin-Elmer Clarus 500) equipped with an FID detector using a high temperature metallic capillary column (PDMS; 6 m × 0.53 mm, 1 μm film thickness). Conversion and selectivity values are expressed as wt% in all the tables and figures.

3. Results and discussion

3.1. Physicochemical properties

3.1.1. Surface area and acidity. The surface area and acidity of the various oxides and mixed oxides including the two spinels, ZnAl₂O₄ and ZnFe₂O₄ are presented in Table 2. The surface areas of the mixtures of Al₂O₃ and ZnO after calcination at 873 K are smaller than those expected for the physical mixtures of Al₂O₃ and ZnO. In fact, they are slightly closer to the values expected for mixtures of Al₂O₃ and ZnAl₂O₄ suggesting that ZnO and Al₂O₃ have reacted to form the ZnAl₂O₄ spinel and the mixtures are probably ZnAl₂O₄ supported on Al₂O₃. In the case of ZnFe₂O₄ it is difficult to analyze the data with reasonable accuracy due to the

small areas involved. Even so, the values are close to those expected for mixtures of Fe₂O₃ and ZnFe₂O₄. The XRD results (section 3.1.2) also confirm the formation of ZnAl₂O₄ and ZnFe₂O₄ in the mixtures.

The pores in ZnAl₂O₄ broaden compared to the γ-Al₂O₃ support with increasing Zn loading in the ZnO–Al₂O₃ system (Table 2). The pore volume/size values of Fe₂O₃ suggest that it has almost a flat surface, but increasing the ZnO loading creates broad pores in the ZnO–Fe₂O₃ system. ZnO has an intermediate pore distribution between ZnAl₂O₄ and ZnFe₂O₄.

The acidities of the samples as measured by the TPD of NH₃ are also presented in Table 2. In order to understand the acidity characteristics of the samples better, the contributions from physical adsorption (if any) and from very weak acid sites (NH₃ desorbing below 350 K) were excluded and the amount of NH₃ that desorbed in the temperature range of 350–800 K is presented in the last column of Table 2. The acidities of ZnAl₂O₄ and ZnFe₂O₄ are 139 and 40 meq g⁻¹, respectively. The acidities of the supports γ-Al₂O₃, Fe₂O₃ and ZnO are 627, 21 and 40 meq g⁻¹, respectively. Though the acidity of ZnAl₂O₄ decreases drastically compared to γ-Al₂O₃, ZnAl₂O₄ contains an almost equal distribution of medium (peak at ~375 K) and strong (peak at ~475 K) acidic sites (Fig. 1). However, in γ-Al₂O₃, medium acidic sites are more dominant than strong acidic sites. The acidities of the supported samples are intermediate to those of the oxides and ZnO; acidity decreases in the case of Al₂O₃ and increases in the case of Fe₂O₃ with increasing ZnO loading. The less than proportionate change in acidity of the supports with ZnO loading suggests that ZnO has interacted strongly with the supports and the supported samples are not physical mixtures of the two oxides.

3.1.2. Powder X-ray diffraction. The XRD patterns of the supported ZnO (5 to 20 wt% of ZnO) samples prepared by impregnation of Zn(NO₃)₂ on γ-Al₂O₃ and Fe₂O₃ and calcination at 873 K are presented in Fig. 2. γ-Alumina exhibits a diffraction pattern with broad, diffuse lines, typical of a microcrystalline material. With increasing loadings of ZnO, the lines due to γ-Al₂O₃ decrease in intensity along with

Table 2 Textural properties and acidity of the samples

Sample	Spinel content (%)	S_{BET} (m ² g ⁻¹)	Pore volume ^a (ml g ⁻¹) [av. pore size ^b ; nm]	Acidity ^c (μmol g ⁻¹) (350–800 K)
ZnAl ₂ O ₄	100.0	62	0.22 [12]	138.7
ZnFe ₂ O ₄	100.0	12	0.10 [21]	40.3
ZnO	—	29	0.10 [15]	69.6
γ-Al ₂ O ₃	—	168	0.35 [8]	626.6
5ZnAl	11.3	133	0.40 [12]	465.5
10ZnAl	22.5	116	0.36 [12]	385.8
20ZnAl	45.0	99	0.30 [12]	292.0
α-Fe ₂ O ₃	—	6	0.06 [40]	21.1
5ZnFe	14.8	7	0.06 [34]	24.4
10ZnFe	29.6	10	0.08 [32]	27.8
20ZnFe	59.2	11	0.10 [32]	28.6

^a From N₂ adsorption at liquid N₂ temperature, $p/p_0 = 0.98$. ^b By BJH method. ^c μmoles of NH₃ desorbed/g of sample in the range 350–800 K.

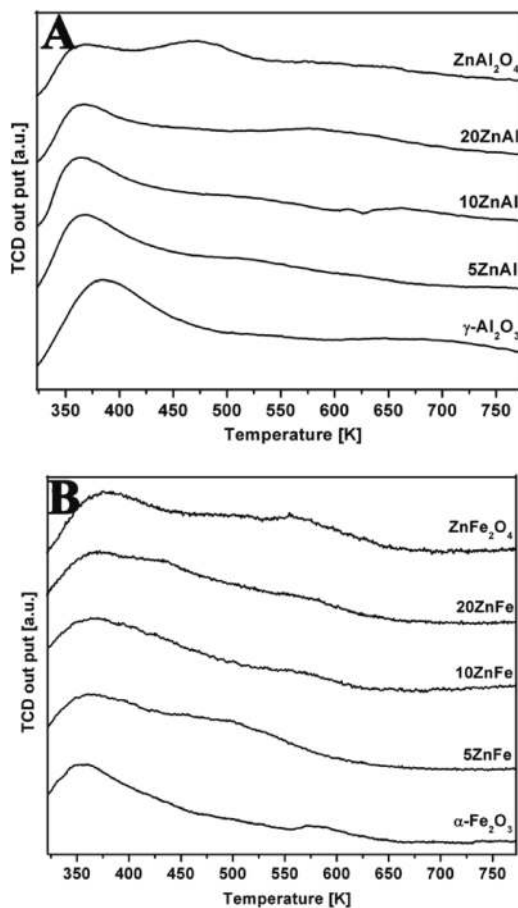


Fig. 1 NH_3 -TPD of (A) $\text{ZnO-Al}_2\text{O}_3$ with different ZnO loadings and ZnAl_2O_4 ; and (B) $\text{ZnO-Fe}_2\text{O}_3$ with different ZnO loadings and ZnFe_2O_4 .

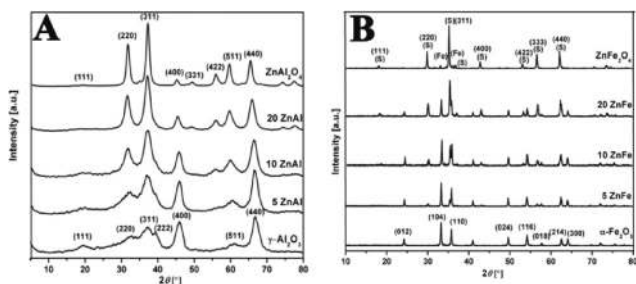


Fig. 2 XRD patterns of (A) $\text{ZnO-Al}_2\text{O}_3$ with different ZnO loadings and ZnAl_2O_4 ; and (B) $\text{ZnO-Fe}_2\text{O}_3$ with different ZnO loadings and ZnFe_2O_4 .

a corresponding increase in the intensity of the spinel phase. A similar behavior is also seen in the patterns of the Fe_2O_3 supported ZnO samples (Fig. 2B). The XRD patterns of ZnAl_2O_4 and ZnFe_2O_4 are typical of the expected spinel phases and are in agreement with JCPDS data (78-1601 and 86-2267). All the diffraction peaks matched the reported patterns. Lines due to individual oxides were barely discernible in the patterns.

3.1.3. UV-Vis spectroscopy. The UV-Vis spectra of ZnO impregnated on Al_2O_3 and Fe_2O_3 along with those of ZnO, Al_2O_3 and Fe_2O_3 are presented in Fig. 3. Assignments of the

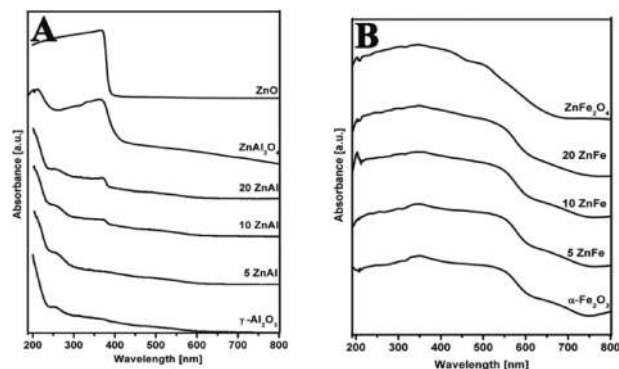


Fig. 3 UV-Vis spectra of (A) ZnO, Al_2O_3 , $\text{ZnO-Al}_2\text{O}_3$ samples and ZnAl_2O_4 , and (B) Fe_2O_3 , $\text{ZnO-Fe}_2\text{O}_3$ samples and ZnFe_2O_4 .

spectral bands (Fig. 3) of the oxides and spinels based on published literature are presented in Table 3. Examining the spectra presented in Fig. 3A, a band at ≤ 215 nm is seen for the $\text{ZnO-Al}_2\text{O}_3$ samples, while ZnAl_2O_4 exhibits a band at ~ 215 nm. A band noticed at ~ 250 nm in the spectra of the Al_2O_3 and $\text{ZnO-Al}_2\text{O}_3$ samples has been attributed by earlier workers to be due to electronic excitations ($\text{O } 2p \rightarrow \text{Al}^{3+} 3s$).^{35,36} Additionally, with increasing Zn content, the band at ~ 360 nm attributed to defect Zn^{2+} sites in ZnAl_2O_4 is found to increase with Zn loading confirming the presence of increasing amounts of the spinel structure in the samples. The spectrum of ZnO shows a very strong and broad absorption below 380 nm with a peak maximum at ~ 360 nm. The similarity in the absorption band is presumably because the Zn^{2+} ions in ZnO and the spinel are both coordinated to O^{2-} ions.³⁵

Increasing the spinel content in the $\text{ZnO-Fe}_2\text{O}_3$ system does not considerably alter the absorption spectra due to the broad absorption of $\alpha\text{-Fe}_2\text{O}_3$ (Fig. 3B) over the entire UV-Vis region (the samples are brown-black). However, small changes are still seen. The broad absorption at ~ 250 nm is due to the $\text{O}^{2-} \rightarrow \text{Fe}^{3+}$ charge transfer in $\alpha\text{-Fe}_2\text{O}_3$. The weak band at ~ 350 nm becomes broader and more intense with increasing Zn loading due to the $\text{O}^{2-} \rightarrow \text{Zn}^{2+}$ charge transfer. Octahedral Fe^{3+} exhibits a weak band at ~ 500 nm due to the crystal field transition which is more clearly observed in the case of ZnFe_2O_4 compared to other samples of the series. Intense absorption in the visible region of $\alpha\text{-Fe}_2\text{O}_3$ is mainly due to various types of CT transitions like metal to metal charge transfer (MT) transitions ($2\text{Fe}^{3+} \rightarrow \text{Fe}^{2+} + \text{Fe}^{4+}$). As Zn atoms are introduced into $\alpha\text{-Fe}_2\text{O}_3$, the decrease in the Fe–O–Fe linkages between adjacent Fe^{3+} cations gradually reduces the intensity of the band at ~ 550 nm along with increasing the formation of ZnFe_2O_4 .³⁷

3.1.4. X-ray photoelectron spectroscopy. X-ray photoelectron spectroscopy (XPS) was used to further investigate ZnAl_2O_4 , ZnFe_2O_4 , and samples of $\text{ZnO-Al}_2\text{O}_3$ and $\text{ZnO-Fe}_2\text{O}_3$ with different ZnO loadings. The Zn $2p_{3/2}$ core level (XPS) and Zn LMM transitions (XAES) of the $\text{ZnO-Al}_2\text{O}_3$ and $\text{ZnO-Fe}_2\text{O}_3$ samples are presented in Fig. 4. Though the 2p core level binding energy (BE) of Zn is insensitive to different chemical

Table 3 Assignment of the major bands in the UV-Vis spectra (Fig. 3) of spinels and oxides

Sample	Absorption maxima ^a (nm)	Assignment/geometry	Reference(s)
ZnAl ₂ O ₄	215–225(s) ~360	Filled O 2p orbitals → empty Al 3s orbitals Filled O 2p → empty Zn 4s orbitals (due to defects)	[34,35]
ZnFe ₂ O ₄	~275, ~360(b) 400–700(b)	Ligand to metal and L → M charge transfer for Oh Fe ³⁺	[36]
Al ₂ O ₃	215–225(b)	Filled O 2p orbitals → empty Al 3s orbitals	[34,35]
Fe ₂ O ₃	250(b) ~350, ~500 and ~550	O ²⁻ to Fe ³⁺ charge transfer Metal to metal charge transfer	[36]
ZnO	200–400(b)	Filled O 2p → empty Zn 4s orbitals	[34,35]

^a Letters in brackets refer to nature of the absorption lines: s, strong and b, broad.

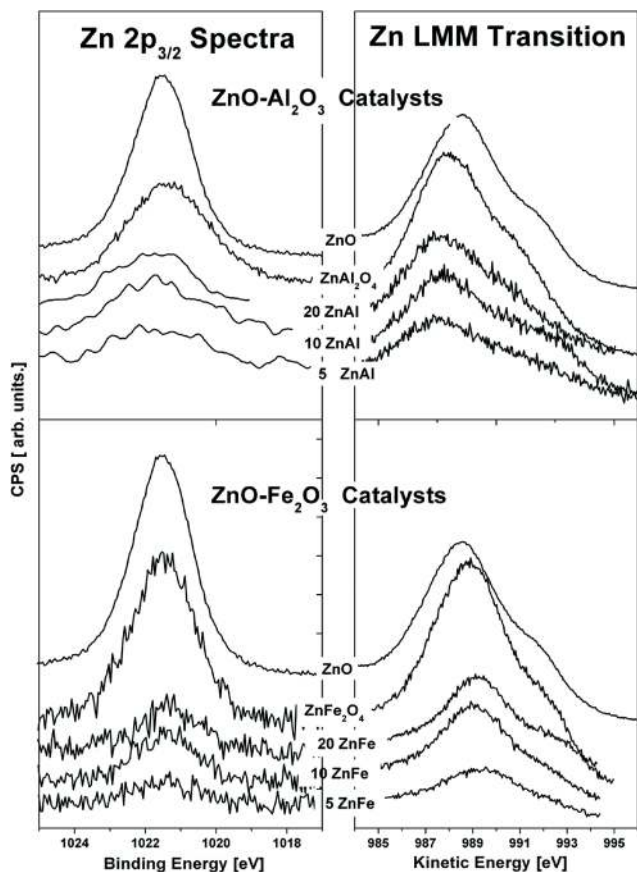


Fig. 4 Zn 2p_{3/2} XP spectra (left panels) and Zn LMM transitions from XAES (right panels) of ZnO–Al₂O₃ and ZnAl₂O₄ (top panels), and ZnO–Fe₂O₃ catalysts and ZnFe₂O₄ (bottom panels). In top and bottom panels, the XPS of Zn 2p_{3/2} (left panels) and XAES of Zn LMM transitions (right panels) of the ZnO samples are also presented for comparison.

states, its modified Auger parameter (α) derived from the Zn 2p_{3/2} BE and Zn LMM Auger lines differentiates the Zn²⁺ and Zn⁰ states.³⁷ From Table 4, the α values of all the catalysts prepared are $\sim 2009 \pm 1$ eV, characteristic of Zn²⁺ ions.³⁸ The full width at half maximum (FWHM) value for the Zn 2p_{3/2} peak of ZnO is lowest due to its unique –O–Zn– environment compared to all the catalysts presented in Table 4 and therefore, in the other catalysts, the Zn²⁺ ions should be

Table 4 Binding energies (in eV) of Zn in ZnO–Al₂O₃ and ZnO–Fe₂O₃, ZnAl₂O₄ and ZnFe₂O₄ (values in parentheses are the FWHM of the peaks in eV)

Sample	Zn 2p _{3/2} ^a eV	Zn LMM ^c eV	Auger parameter, α eV
5ZnAl	1021.0 (3.8 ^b)	987.7	2008.7
10ZnAl	1021.6 (3.1)	987.8	2009.4
20ZnAl	1021.8 (2.6)	987.8	2009.6
ZnAl ₂ O ₄	1021.4 (2.7)	987.9	2009.3
ZnO	1021.5 (2.0)	988.5	2010.0
5ZnFe	1021.5 (2.3)	989.2	2010.7
10ZnFe	1021.4 (2.0)	989.2	2010.6
20ZnFe	1021.3 (2.1)	989.2	2010.5
ZnFe ₂ O ₄	1021.4 (2.0)	989.0	2010.4

^a Binding energy. ^b Full width at half maximum. ^c Kinetic energy.

present in spinel or supported spinel phase where different environments around Zn are possible as evidenced by the XRD results (section 3.1.2.). With increasing loadings of ZnO in both the systems, the difference in environment vanishes until it reaches stoichiometric spinel composition. Moreover, at lower loadings of ZnO, the spinels might be present as smaller crystallites and this may be the reason for the higher FWHM values. A Zn LMM transition is observed at the kinetic energy of 987.8 ± 0.1 eV for ZnO–Al₂O₃, at 989.0 ± 0.1 eV for ZnO–Fe₂O₃ and 988.5 eV for ZnO. The higher value for ZnO–Fe₂O₃ shows that the Zn²⁺ ions in ferrite are richer in electrons than in the aluminates and ZnO. A shoulder in the Zn LMM transition at ~ 991 eV for the ZnO–Al₂O₃ samples and ~ 992 eV for the ZnO–Fe₂O₃ samples is found to emerge with increasing Zn loadings in both systems. Strohmeier and Hercules³² have suggested that this is due to l-s coupling of the Zn atom in the oxide environment. The l-s coupling is strongest for ZnO compared to the other catalysts.

The XP spectra in the valence band (VB) region of the ZnO–Al₂O₃ and ZnO–Fe₂O₃ samples are presented in Fig. 5. The main VB appearing at 11 eV and 10 eV, respectively, in the top and bottom panels in the figure is associated with Zn 3d; the Zn 3d band of ZnO appears at 10.3 eV. Note that the LMM Auger transition of Zn involves Zn 3d (L) and Zn 2p (M) electrons. In the ZnO system, the lowest valence band lies below the Zn 3d level.³⁸ Other bands at 7 eV in the top

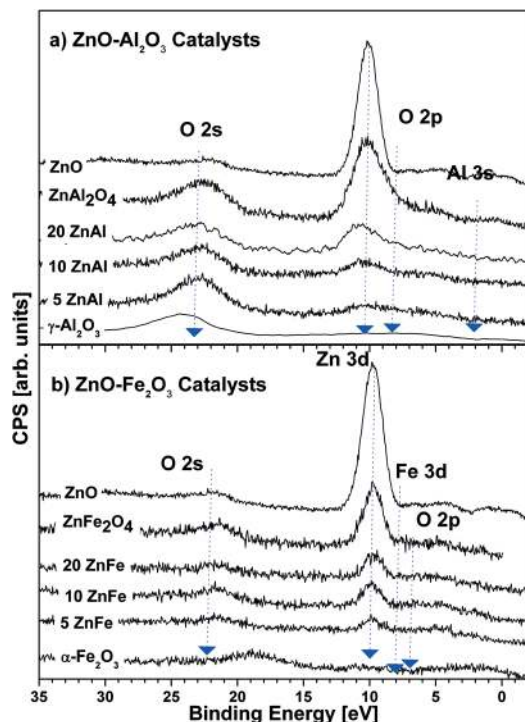


Fig. 5 Valence band (VB) spectra from XPS studies of (a) ZnO–Al₂O₃ and (b) ZnO–Fe₂O₃ samples with corresponding stoichiometric spinels. VB spectra of γ -Al₂O₃ and Fe₂O₃ have been rescaled ($\times 10$) to fit in the figure.

panel and 8 eV in both panels are due to Fe 3d and O 2p levels.¹⁶ Particularly, the Fe 3d band appears to be very weak in all the catalysts of the ZnO–Fe₂O₃ system including α -Fe₂O₃ probably due to the spin-forbidden transition of Fe³⁺ ions in the d⁵ configuration. The band for the O 2s orbital appears at ~23 eV for the ZnO–Al₂O₃ samples and at ~22 eV for the ZnO–Fe₂O₃ samples. The higher binding energy of the O 2s band of ZnO–Al₂O₃ compared to ZnO–Fe₂O₃ is due to the greater ionic nature of the Al–O bonds than the Fe–O bonds.^{39–42} From the XVB spectra it is clear that the surface valence band is dominated by the Zn 3d orbitals in both systems and the intensity of the Zn 3d peak increases with increasing Zn content in both systems. From the valence band spectra, it was concluded that the Zn 3d electrons are actively involved in spinel formation for both systems and likely to take part to a major extent in the electronic excitation of the spinels (ZnAl₂O₄ and ZnFe₂O₄) and, therefore, their catalytic activity.

The XP spectra of the O 1s region of the ZnO–Al₂O₃ and ZnO–Fe₂O₃ samples are presented in Fig. 6. At Zn loadings of up to 20%, the O 1s peak is observed at 531.2 ± 0.2 eV for ZnO–Al₂O₃ and at 530 ± 0.2 eV for Zn–Fe₂O₃. The O 1s peaks of adsorbed water (–OH₂) and basic hydroxide (–OH), generally observed at 533.2 ± 0.1 eV and 532.2 ± 0.1 eV, respectively,^{43,44} are also seen in the spectra (Fig. 6B).

These peaks are, however, relatively less intense in the ZnO–Al₂O₃ samples which may be due to a relatively small BE difference between the basic hydroxide group and the main O 1s peak from the Al₂O₃ support. From Fig. 6B, it is

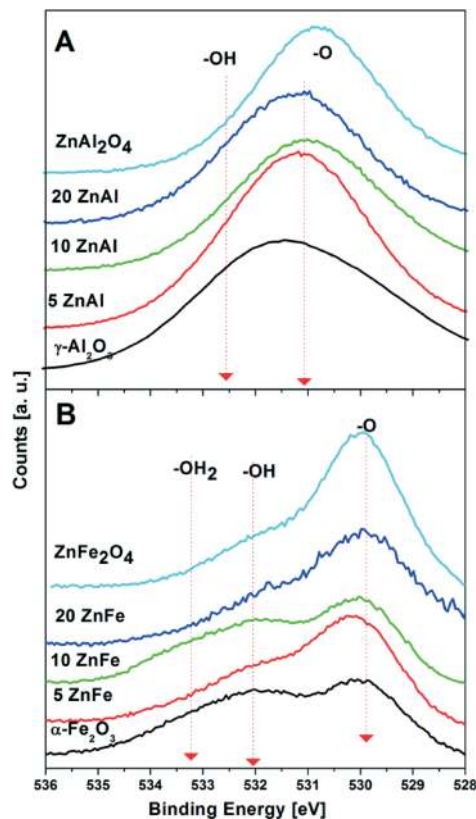


Fig. 6 O 1s spectra from XPS studies of (A) ZnO–Al₂O₃ and (B) ZnO–Fe₂O₃ with their corresponding stoichiometric spinels. The O 1s spectrum of ZnO is also given in the figure for comparison.

clear that the intensity of the peaks due to adsorbed water and the basic hydroxide group decreases as the spinel phase increases. This might be due to the hydrophobic nature of the stoichiometric spinels.

3.1.5. IR spectroscopy in DRIFT mode. The IR spectra in DRIFT mode for the spinels were recorded at a sample temperature of 673 K under a nitrogen atmosphere, in order to avoid interference from –OH vibrations due to moisture, and are presented in Fig. 7. As the evolution of the spinel phase with increasing ZnO loadings was clearly observed by XRD, UV-Vis and XPS spectra, we concentrated on the –OH group region ($4000\text{--}3000\text{ cm}^{-1}$) of the IR spectra to understand the nature of the surface hydroxyl groups in the spinel-type oxides in the present study. For γ -Al₂O₃ (Fig. 7A), three distinct bands were observed around 3728 , 3678 and 3560 cm^{-1} in the “–OH” region. The first peak corresponds to terminal –OH groups mainly located on octahedrally coordinated Al³⁺ and the other two distinct bands were assigned to bridging –OH and triply-bridging –OH.⁴⁵ A new band appearing at $\sim 3680\text{ cm}^{-1}$ (ZnAl₂O₄) is due to hydroxyl groups on the tetrahedrally coordinated Zn²⁺ with increasing Zn wt% loadings into the alumina.⁴⁶ However, a new band forming at 3580 cm^{-1} because of the merging of bands at 3678 and 3560 cm^{-1} might be attributed to the formation of Zn containing spinels and a new bridging group, Zn–O–Al, on the surface. In the case of Fe₂O₃, the IR spectra in Fig. 7B exhibit

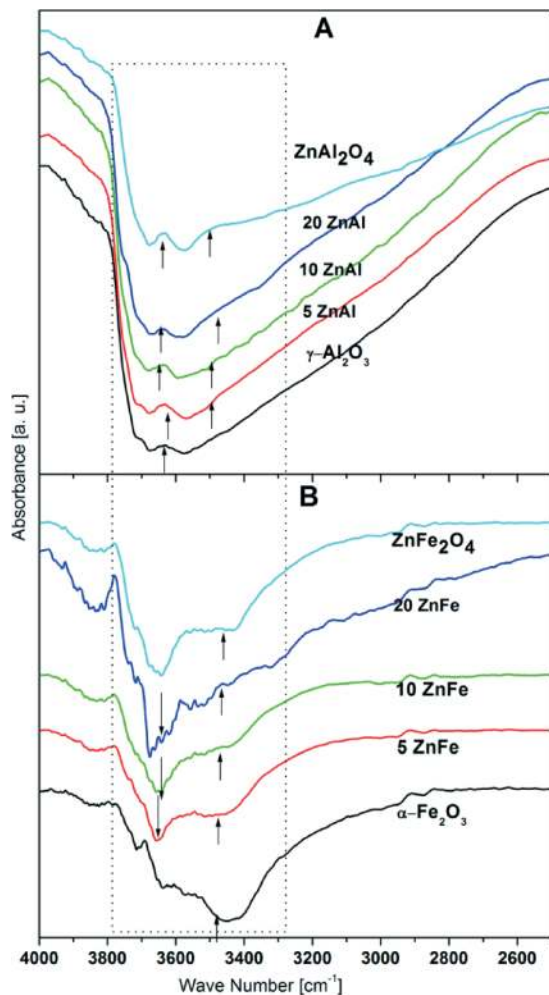


Fig. 7 DRIFT IR spectra of (A) ZnO, Al₂O₃, ZnO–Al₂O₃ samples and ZnAl₂O₄, and (B) Fe₂O₃, ZnO–Al₂O₃ samples and ZnFe₂O₄.

multiple bands due to different types of –OH groups. The bands at 3660 and 3675 cm⁻¹ are attributed to the hydroxyl groups on octahedral Fe³⁺. A weak band at ~3719 cm⁻¹ due to non vacant or near cation vacancy is observed for the terminal –OH group which lies on tetrahedral Fe³⁺ like pure Fe₂O₃.⁴⁶ The bands for the bridging and triply bridging –OH group appear at ~3550 cm⁻¹ and at ~3450 cm⁻¹ (a broad peak), respectively.⁴⁶ Similar to the ZnAl₂O₄ samples, the intensity of the band at ~3680 cm⁻¹ increases with increasing ZnO content due to the newly formed –OH groups on tetrahedral Zn²⁺. Consequently, in ZnAl₂O₄ and ZnFe₂O₄, the intensity of the various hydroxyl groups decreases with increasing ZnO percentage *i.e.* the formation of the spinel phase. This indicates the formation of new hydrophobic sites on the spinel type oxide surface.

3.2. Studies on transesterification of vegetable oils

Evaluation of the catalytic activity of the different ZnO loaded Al₂O₃ and Fe₂O₃ samples in the transesterification of vegetable oils with methanol was carried out in a SS batch reactor

using three different vegetable oils; sunflower, Jatropha and waste oil.

The transesterification activities of the supported spinel catalysts are given in Fig. 8. The conversion of sunflower oil (triglycerides, TG) and the individual selectivity for the intermediates, the di and monoglycerides (DG and MG), and the final product FAME are presented in the figures as a function of % ZnO loading. The last point in the figures is for the stoichiometric spinel prepared by the coprecipitation method. It can be seen that activity increases linearly with ZnO content, the linearity being higher in the case of the ZnO–Fe₂O₃ samples. In the case of the pure spinels, the (nearly) only product of the reaction is a mixture of fatty acid methyl esters (FAME). The other expected products, *viz.* the diglycerides (DG) and monoglycerides (MG) were together less than 0.5 wt% in the product. More of these intermediates, especially the MG, are found in the case of the less active samples. However, the amounts of these compounds are less

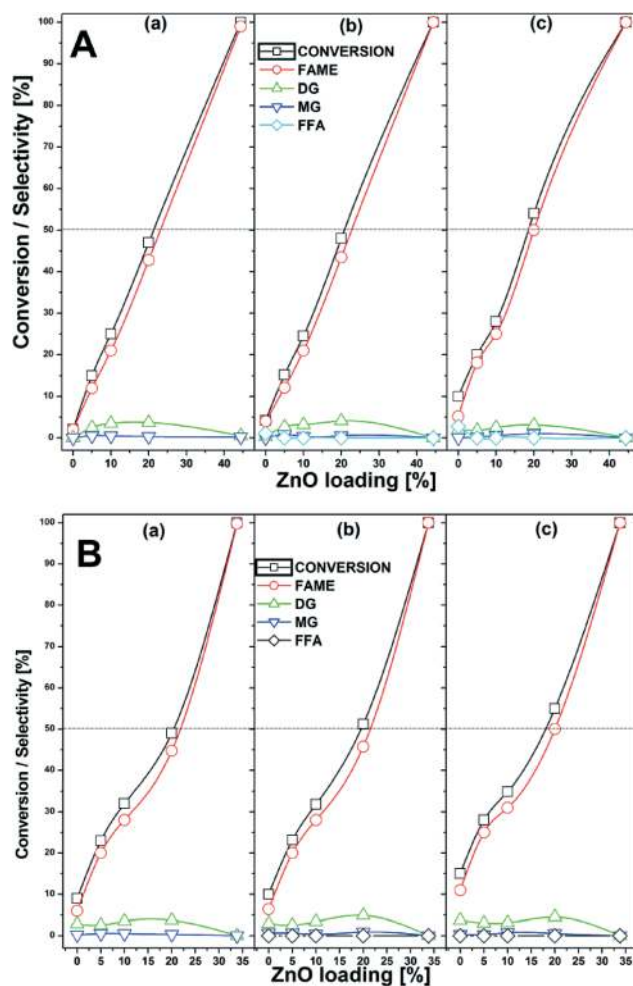


Fig. 8 Influence of ZnO loading on transesterification activity of [A] ZnO–Al₂O₃ samples: (a) sunflower oil, (b) waste cooking oil and (c) Jatropha oil (conditions: catalyst, 1 g; 453 K; oil, 20 g; MeOH/oil (mole), 9; run duration, 10 h). [B] ZnO–Fe₂O₃ samples: (a) sunflower oil, (b) waste cooking oil and (c) Jatropha oil (conditions: catalyst, 1 g; 453 K; oil, 20 g; MeOH/oil (mole), 9; run duration, 10 h).

than 4% in all the products. It appears from these studies that the Zn spinel phase is mainly responsible for the activity of these calcined mixed oxides. The imaginary lines drawn in Fig. 8 clearly indicate that the transesterification activity is better for 5, 10 and 20% loadings of ZnO of ZnO-Fe₂O₃ samples than for the ZnO-Al₂O₃ samples. Both the catalysts can be used for at least 5 cycles without noticeable loss in activity and can be used for a fixed bed run of at least 48 hours, according to our present study. The detailed results of the transesterification activity studies on the ZnFe₂O₄ spinel catalyst with other spinel catalysts is discussed elsewhere.³³

3.3. Structure–activity correlations

The characterization studies reported earlier revealed the formation of spinel-type phases in the samples, making them essentially spinels supported on Al₂O₃ and Fe₂O₃. The XRD studies revealed the formation of increasing amounts of the spinel species with increasing Zn-loading, while UV-Vis and XPS studies also provided indirect evidence for the formation of the spinel phases. The information on the surface hydroxyl groups of the mixed spinel-type oxides in the present study with XPS (O 1s region) and DRIFT-IR studies revealed the creation of hydrophobic sites with increasing ZnO content. Indeed, these hydrophobic sites facilitate the rapid adsorption of TG, which is also hydrophobic.⁴⁷

Plots of the amount of Zn loaded in the ZnO-Al₂O₃ and ZnO-Fe₂O₃ samples vs. their catalytic activity, relative bulk spinel content (as established by intensity of the 311 peak in XRD) and relative intensity of Zn 2p measured by XPS are presented in Fig. 9. Nearly linear relationships between Zn-loading, spinel-content, surface Zn-intensity (XPS) and activity (sunflower oil conversion) are noticed (Fig. 9) confirming the role of the spinel phase in the catalytic activity. Relative intensity values (XRD and XPS) were calculated with respect to the stoichiometric spinels prepared by the co-precipitation method (the last point in the figures). In the case of the ZnO-Fe₂O₃ samples the relative surface Zn concentrations from XPS more closely follow the transesterification activity than that for the ZnO-Al₂O₃ samples, suggesting a direct involvement of the spinel phase in the activity of the former compared to the later. From the characterization studies, it is clear that the ZnO-Al₂O₃ catalysts are highly porous with a

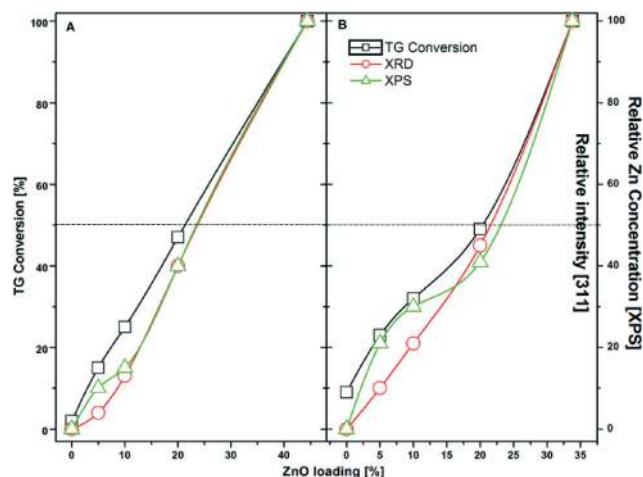


Fig. 9 Relationships between ZnO loading, transesterification activity, relative spinel-content from XRD peak (311) intensity and relative intensity of Zn 2p peak in XPS for (A) ZnO-Al₂O₃ and (B) ZnO-Fe₂O₃ (conditions: catalyst, 1 g; 453 K; sunflower oil, 20 g; MeOH/oil (mole), 9; run duration, 10 h).

high surface area and ZnO-Fe₂O₃ catalysts are almost flat with a low surface area. Therefore the higher transesterification activity of the ZnO-Al₂O₃ catalysts than that expected from the surface Zn concentrations must be due to the higher surface area and porous nature of them; on the other hand, the activity of the ZnO-Fe₂O₃ catalysts can be attributed to the surface concentrations of Zn²⁺ ions.

The activity of the different oxides and the two spinels are compared (on a wt and area basis) in Table 5. The conversions recorded on the two spinels, ZnAl₂O₄ and ZnFe₂O₄, at a run time of 10 h are similar, being about 100%. However, their activities are different when they are calculated on an area basis. There is no direct relationship of surface area and acidity with the transesterification activity as can be seen in Table 5. Comparing the specific activities calculated on a surface area basis at a run time of 2 h, it is found that ZnFe₂O₄ is much more active (191 μmol m⁻² h⁻¹) than ZnAl₂O₄ (37 μmol m⁻² h⁻¹). Though the activity of ZnO is also fairly large (72 μmol m⁻² h⁻¹), it is, however, found to leach into the reaction medium during the reaction, and hence is not suitable as a catalyst. It is interesting to point out here that the specific activities of ZnAl₂O₄, ZnFe₂O₄ and ZnO for

Table 5 Comparison of activity of different spinels and oxides

Sample	Surface area ^a (m ² g ⁻¹)	Acidity μmol g ⁻¹ (350–800 K)	Activity (% conversion) at run time		Specific activity ^b (μmol m ⁻² h ⁻¹) at run time	
			10 h	2 h	10 h	2 h
ZnAl ₂ O ₄	62	138.7	100	20	35	37
ZnFe ₂ O ₄	12	40.3	100	21	190	191
ZnO	29	69.6	98	17	79	72
γ-Al ₂ O ₃	168	626.6	2	—	0.2	—
α-Fe ₂ O ₃	6	21.1	9	2	33	38

^a From N₂ adsorption, using BET equation. ^b TG converted per mol per unit surface area per gram of catalyst (conditions: catalyst, 1 g; 453 K; sunflower oil, 20 g; MeOH/oil (mole), 9).

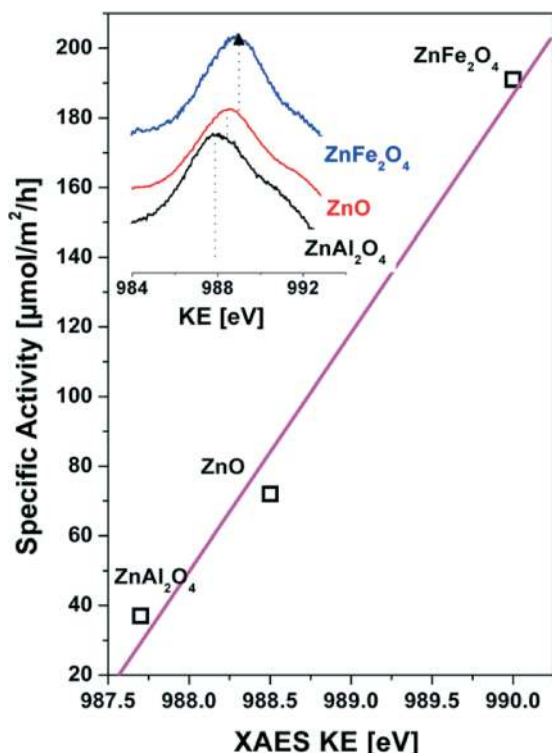


Fig. 10 The linear relationship of Zn LMM (XAES) transitions with the specific transesterification activities of ZnAl_2O_4 , ZnO and ZnFe_2O_4 . The inset shows the corresponding Zn LMM transitions of ZnAl_2O_4 , ZnO and ZnFe_2O_4 .

the transesterification reaction increase in the same order of Zn LMM values, *i.e.*, the electron density on Zn^{2+} ions (ZnAl_2O_4 (987.7 ± 0.1 eV) < ZnO (988.5 eV) < ZnFe_2O_4 (990 ± 0.1 eV), section 3.1.4.) (see, Fig. 10). The activities of the pure oxides are much lower, sunflower oil conversion being 9 and 2% at 10 h, respectively, over Fe_2O_3 and Al_2O_3 , though due to the low surface area of Fe_2O_3 , its specific activity is, however, large ($35 \mu\text{mol m}^{-2} \text{h}^{-1}$).

Activation energy values based on biodiesel conversion gave an E_a value of $14.5 \text{ kcal mol}^{-1}$ for ZnAl_2O_4 and 14 kcal mol^{-1} for ZnFe_2O_4 for sunflower oil (Fig. S1, in ESI†) suggesting the absence of diffusion effects under the experimental conditions used. Similar values have been reported by earlier workers for the acid catalyzed transesterification of vegetable oils.⁴⁸ This further proves that the ZnFe_2O_4 surface more considerably reduces the activation energy of the reaction than ZnAl_2O_4 even though it has a flat surface and lower surface area as it has the electron rich Zn-ions.

4. Conclusions

The studies herein reveal that when $\text{Zn}(\text{NO}_3)_2$ is impregnated on Al_2O_3 and Fe_2O_3 and calcined at 873 K, crystalline spinel phases of ZnAl_2O_4 and ZnFe_2O_4 are readily formed on the surface. Both ZnAl_2O_4 and ZnFe_2O_4 are active in the transesterification of vegetable oils (sunflower, Jatropha and waste cooking oils). A linear relationship between Zn-spinel

content and transesterification activity is obtained for the supported catalysts. XVB (X-ray valence band) studies reveal that the surface valence bands of the two spinels are dominated by Zn 3d orbitals and the intensity of the Zn 3d peak increases with increasing Zn content in the supported samples; this suggests that Zn 3d electrons are likely to take part to a major extent in the electronic excitation of the spinels (ZnAl_2O_4 and ZnFe_2O_4) during the reaction and, presumably therefore, their transesterification activity. The electron densities of Zn-ions play a crucial role in the activity of the examined spinel samples.

Acknowledgements

The authors thank Head, NCCR, IIT Madras and DST, New Delhi.

Notes and references

- Z. Helwani, M. R. Othman, N. Aziz, J. Kim and W. J. N. Fernando, *Appl. Catal., A*, 2009, **363**, 1–10.
- M. Di Serio, R. Tesser, L. Pengmei and E. Santacesaria, *Energy Fuels*, 2008, **22**, 207–217.
- G. R. Peterson and W. P. Scarrah, *J. Am. Oil Chem. Soc.*, 1984, **61**, 1593–1597.
- E. Lotero, Y. Liu, D. E. Lopez, K. Suwannakaran, D. A. Bruce and J. G. Goodwin Jr., *Ind. Eng. Chem. Res.*, 2005, **44**, 5353–5363.
- D.-W. Lee, Y.-M. Park and K.-W. Lee, *Catal. Surv. Asia*, 2009, **13**, 63–77.
- R. Stern, G. Hillion, J.-J. Rouxel and S. Leporq, *US Pat.* 5908946, 1999, to Institut Francais du Petrole.
- L. Bournay, G. Hillion, P. Boucot, J.-A. Chodorge, C. Bronner and A. Forestiere, *US Pat.* 6878837, 2005, to Institut Francais du Petrole.
- W. R. Cares and J. W. Hightower, *J. Catal.*, 1971, **23**, 193–203.
- F. L. Peltier, P. Chaumette, J. Saussey, M. M. Bettahar and J. C. Lavalley, *J. Mol. Catal. A: Chem.*, 1998, **132**, 91–100.
- R. Roesky, J. Weiguny, H. Bestgen and U. Dingerdissen, *Appl. Catal., A*, 1999, **176**, 213–220.
- H. Grobowska, W. Mista, J. Trawczyz and M. Zawadzki, *Appl. Catal., A*, 2001, **220**, 207–213.
- T. E. Nabarawy, A. A. Attia and M. N. Alaya, *Mater. Lett.*, 1995, **24**, 319–325.
- G. Aguilar-Rios, M. Valenzuela, P. Salals, M. Armendariz, P. Bosh, G. Del Toro, R. Silva, V. Bertin, S. Castillo, A. Ramirez-soliz and I. Schiftler, *Appl. Catal., A*, 1995, **127**, 65–75.
- X. Li, Z. Zhu, Q. Zhao and L. Wang, *J. Hazard. Mater.*, 2011, **186**, 2089–2096.
- L. Zhang, J. Yan, M. Zhou, Y. Yang and Y.-N. Liu, *Appl. Surf. Sci.*, 2013, **268**, 237–245.
- M. Vijayaraj and C. S. Gopinath, *J. Catal.*, 2006, **241**, 83–95.
- K. Sreekumar and S. Sugunan, *Appl. Catal., A*, 2002, **230**, 245–251.

- 18 P. T. A. Santos, A. C. F. Costa and H. M. C. Andrade, *Mater. Sci. Forum*, 2012, 727–728, 1290–1295.
- 19 F. M. Moghadden, M. Doulabi and H. Saeidian, *Sci. Iran., Trans. C*, 2012, 19, 1597–1600.
- 20 H. Lee, J. C. Jung, H. Kim, Y.-M. Chung, T. J. Kim, S. J. Lee, S.-H. Oh, Y. S. Kim and I. K. Song, *Catal. Lett.*, 2009, 131, 344–349.
- 21 H. Armendariz, G. Aguilar-Rios, P. Salas, M. A. Valenzuela, I. Schifter, H. Arrioka and N. Nava, *Appl. Catal., A*, 1992, 92, 29–38.
- 22 R. Dom, R. Subasri, N. Y. Hebalkar, A. S. Chary and A. S. Borse, *RSC Adv.*, 2012, 2, 12782–12791.
- 23 G. Fan, J. Tong and F. Li, *Ind. Eng. Chem. Res.*, 2012, 51, 13639–13647.
- 24 X. Xu, A. K. Azad and J. T. S. Irvine, *Catal. Today*, 2013, 199, 22–26.
- 25 J.-P. Jacobs, A. Maltha, J. G. H. Reintjes, J. Drimal, V. Ponc and H. Brongersma, *J. Catal.*, 1994, 147, 294–300.
- 26 N. Nava, J. P. Jacobs, A. Garcla, J. J. W. M. Rosink, M. A. Valenzuela, L. J. Van Ijzendoorn and H. H. Brongersma, *J. Radioanal. Nucl. Chem. Lett.*, 1996, 212, 431–443.
- 27 L. Bournay, D. Casanave, B. Delfort, G. Hillion and J. A. Chodorge, *Catal. Today*, 2005, 106, 190–192.
- 28 V. Pugnet, S. Maury, V. Coupard, A. Dandeu, A.-A. Quoineaud, J.-L. Bonneau and D. Tichit, *Appl. Catal., A*, 2010, 374, 71–78.
- 29 W. Jiang, H.-F. Lu, T. Qi, S.-I. Yan and B. Liang, *Biotechnol. Adv.*, 2010, 28, 620–627.
- 30 Q. Liu, L. Wang, C. Wang, W. Qu, Z. Tian, H. Ma, D. Wang, B. Wang and Z. Xu, *Appl. Catal., B*, 2013, 136–137, 210–217.
- 31 C. T. Alves, A. Oliveira, S. A. V. Carneiro, A. G. Silva, H. M. C. Andrade, S. A. B. Vieira de Melo and E. A. Torres, *Fuel Process. Technol.*, 2013, 106, 102–107.
- 32 B. R. Strohmeier and D. M. Hercules, *J. Catal.*, 1984, 86, 266–279.
- 33 T. M. Sankaranarayanan, A. Pandurangan, M. Banu and S. Sivasanker, *Appl. Catal., A*, 2011, 409–410, 239–247.
- 34 T. M. Sankaranarayanan, R. Vijaya Shanthi, K. Thirunavukkarasu, A. Pandurangan and S. Sivasanker, *J. Mol. Catal. A: Chem.*, 2013, 379, 234–242.
- 35 S. K. Sampath and J. F. Cordaro, *J. Am. Ceram. Soc.*, 1998, 81, 649–654.
- 36 S. Mathur, M. Veith, M. Haas, H. Shen, N. Lecerf, V. Huch, S. Hufner, R. Haberkorn and H. P. Beck, *J. Am. Ceram. Soc.*, 2001, 84, 1921–1928.
- 37 L. G. J. de Haart and G. Blasse, *J. Electrochem. Soc.*, 1985, 132, 2933–2938.
- 38 G. Moretti, *J. Electron Spectrosc. Relat. Phenom.*, 1998, 95, 95–144.
- 39 L. Ley, R. A. Pollak, F. R. McFecly, S. I. Kowalczyk and D. A. Shirley, *Phys. Rev. B: Solid State*, 1974, 9, 600–621.
- 40 R. H. French, *J. Am. Ceram. Soc.*, 1990, 73, 471–489.
- 41 Y. Yourdshahyan, C. Ruberto, M. Halvarsson, L. Bengtsson, V. Langer and B. I. Lundqvist, *J. Am. Ceram. Soc.*, 1999, 82, 1365–1380.
- 42 G. Rollmann, A. Rohrbach, P. Entel and J. Hafner, *Phys. Rev. B: Condens. Matter Mater. Phys.*, 2004, 69, 165107–165119.
- 43 K. Kotsis and V. Staemmler, *Phys. Chem. Chem. Phys.*, 2006, 8, 1490–1498.
- 44 J. L. Junta-Rosso and M. F. Hochella Jr, *Geochim. Cosmochim. Acta*, 1996, 60, 305–314.
- 45 A. A. Tsyganenko, K. S. Smirnov, A. M. Rzhetskij and P. P. Mardilovich, *Mater. Chem. Phys.*, 1990, 26, 35–46.
- 46 G. Busca, V. Lorenzelli, G. Ramis and R. J. Willey, *Langmuir*, 1993, 9, 1492–1499.
- 47 D. M. Reinoso, D. E. Damiani and G. M. Tonetto, *Appl. Catal., B*, 2014, 144, 308–316.
- 48 B. Freedman, R. O. Butterfield and E. H. Pryde, *J. Am. Oil Chem. Soc.*, 1986, 63, 1375–1380.